Earth and Planetary Science Letters 281 (2009) 59–69

Contents lists available at ScienceDirect

Earth and Planetary Science Letters

journal homepage: www.elsevier.com/locate/epsl

Modeling seismic swarms triggered by aseismic transients

Andrea L. Llenos [a,*], Jeffrey J. McGuire [b], Yosihiko Ogata [c]

[a] *MIT/WHOI Joint Program, 77 Massachusetts Ave., 54-710, Cambridge, MA 02139, USA*
[b] *Woods Hole Oceanographic Institution, MS #24, Woods Hole, MA 02543, USA*
[c] *Institute of Statistical Mathematics, Minami-Azabu 4-6-7, Minato-Ku, Tokyo, 106-8569, Japan*

ARTICLE INFO

Article history:
Received 14 August 2008
Received in revised form 30 January 2009
Accepted 6 February 2009
Available online 9 March 2009

Editor: T.M. Harrison

Keywords:
earthquake swarms
aseismic deformation
ETAS model
rate–state model
triggering

ABSTRACT

The rate of earthquake occurrence varies by many orders of magnitude in a given region due to variations in the stress state of the crust. Our focus here is on variations in seismicity rate triggered by transient aseismic processes such as fluid flow, fault creep or magma intrusion. While these processes have been shown to trigger earthquakes, converting observed seismicity variations into estimates of stress rate variations has been challenging. Essentially aftershock sequences often obscure changes in the background seismicity rate resulting from aseismic processes. Two common approaches for estimating the time dependence of the underlying driving mechanisms are the stochastic Epidemic Type Aftershock Sequence model (ETAS) [Ogata, Y., (1988), Statistical models for earthquake occurrences and residual analysis for point processes, J. Am. Stat. Assoc., 83, 9–27.] and a physical approach based on the rate- and state-model of fault friction [Dieterich, J., (1994), A constitutive law for rate of earthquake production and its application to earthquake clustering, J. Geophys. Res., 99, 2601–2618.]. The models have different strengths that could be combined to allow more quantitative studies of earthquake triggering. To accomplish this, we identify the parameters that relate to one another in the two models and examine their dependence on stressing rate. A particular conflict arises because the rate–state model predicts that aftershock productivity scales with stressing rate while the ETAS model assumes that it is time independent. To resolve this issue, we estimate triggering parameters for 4 earthquake swarms contemporaneous with geodetically observed deformation transients in various tectonic environments. We find that stressing rate transients increase the background seismicity rate without affecting aftershock productivity. We then specify a combined model for seismicity rate variations that will allow future studies to invert seismicity catalogs for variations in aseismic stressing rates.

1. Introduction

Earthquake swarms are time periods of elevated seismicity rate that lack an obvious mainshock, and they are one of the clearest signals that many processes in the crust have variations on time scales of hours to days. The most common time periods of increased seismicity rate are the aftershock sequences that follow all large crustal earthquakes and generally decay away according to Omori's empirical law (Utsu, 1961). The term swarm has been used qualitatively by seismologists for nearly a century to describe temporal clusters of earthquakes that are not well described by Omori's law (Richter, 1958). Swarms are common in volcanic regions and have been explained as resulting from the stress perturbations during magma intrusions (e.g., Einarsson and Brandsdóttir, 1980; Dieterich et al., 2000; Smith et al., 2004) as well as from the movements of volatiles such as CO_2 (e.g., Prejean et al., 2003; Hainzl and Ogata, 2005). Similarly, earthquake swarms are common in regions of aqueous fluid flow such as geothermal areas (Hill et al., 1975) and during hydrofracture experiments (Audigane et al., 2002; Shapiro et al., 2005; Bourouis and Bernard, 2007). Thus, a clear intuition has developed that swarms are driven by aseismic events that temporarily modify the stress state within the crust. Toda et al. (2002) recently formalized this hypothesis for a swarm of ~7000 earthquakes in the Izu islands that was associated with a large dike intrusion. They demonstrated that the seismicity rate varied spatially in proportion to the variations in the stress rate increase caused by the magmatic intrusion.

Recently a number of earthquake swarms have been found in association with times when a fault undergoes a large amount of slip without radiating seismic waves. These events are often termed slow earthquakes, silent earthquakes or creep events and require high quality geodetic data to detect owing to their lack of seismic radiation. Swarms triggered by such aseismic fault slip have been found in a number of tectonic regions. Ozawa et al. (2007) found swarms coincident with repeating slow earthquakes on the subduction zone thrust interface offshore of central Honshu. In these cases the slow event typically has a moment magnitude of M_w~6.5 while the largest

* Corresponding author. Tel.: +1 617 324 3887; fax: +1 508 457 2150.
E-mail addresses: allenos@mit.edu (A.L. Llenos), jmcguire@whoi.edu (J.J. McGuire), ogata@ism.ac.jp (Y. Ogata).

0012-821X/$ – see front matter © 2009 Elsevier B.V. All rights reserved.
doi:10.1016/j.epsl.2009.02.011

earthquakes in the swarm are $M_w \sim 4$, indicating that the vast majority of fault motion happens aseismically and only a few small patches fail seismically. A similar behavior was observed for a continental strike-slip fault by Lohman and McGuire (2007) in the Salton Trough region of California, where a swarm of ~1000 $M_w < 5.1$ earthquakes was triggered by a M_w 5.7 slow event. Wolfe et al. (2007) found swarms of ~10–50 earthquakes associated with slow events on a detachment fault beneath Kilauea's south flank. Similarly a swarm of ~1700 earthquakes in a volcanic region in Japan was also found to be associated with a much larger aseismic slip transient on reverse faults (Takada and Furuya, in review). Collectively these studies indicate that relatively modest earthquake swarms with events in the magnitude 4–5 range often result from much larger aseismic slip transients that generate microseismicity by loading neighboring regions of a fault system. Additionally, surveys of seismicity catalogs by Vidale et al. (2006) and Vidale and Shearer (2006) have found that swarms are widespread phenomena in California and Japan and often cover an unusually large area for their cumulative seismic moment, a property that corresponds well with the low stress drops observed for shallow aseismic creep events (Brodsky and Mori, 2007).

It is difficult to untangle the contribution of any time-dependent driving process from an earthquake catalog because of the preponderance of standard earthquake–earthquake triggering (e.g., aftershock sequences). Given a triggering model that utilizes an aftershock triggering exponent α, the Gutenberg–Richter parameter b, and an offset $\Delta M_{\mathrm{after}}$ describing the magnitude difference between a mainshock and its largest probable aftershock, the branching ratio $n = 10^{-\alpha\Delta M_{\mathrm{after}}} b/(b-\alpha)$ describes the average fraction of a catalog consisting of triggered earthquakes (Helmstetter and Sornette, 2002; Boettcher and Jordan, 2004). Using values of $\alpha \approx 0.8$, $b \approx 1$ and $\Delta M_{\mathrm{after}} \approx 0.9$ that are consistent with southern California seismicity data (Helmstetter, 2003; Helmstetter and Sornette, 2003), up to roughly 90% of earthquakes in this region are triggered by other earthquakes. This number, however, is highly dependent on the value for α, which is likely between 0.8 and 1, and the parameter $\Delta M_{\mathrm{after}}$ can also range from 0.9 to 1.2 (Helmstetter, 2003; Helmstetter and Sornette, 2003). Yet even with these ranges of values, around 60–90% of earthquakes in the catalog are aftershocks. Thus, even when some aseismic process is triggering an elevated rate of seismicity, that seismicity will generate its own aftershock sequences, which will ultimately comprise a significant fraction of the earthquake catalog. There are currently two main approaches to analyzing seismicity rate variations: stochastic models such as the Epidemic Type Aftershock Sequence (ETAS) model (Ogata, 1988), and physical models such as the rate- and state-dependent friction model (Dieterich, 1994).

The ETAS stochastic model is an effective way to detect anomalous seismicity rates. By modeling earthquake occurrence as a point process described by just a few optimizable parameters, the model can detect time periods that are not well described by a stationary stochastic process (McGuire et al., 2005). Recently, studies have utilized a space–time version of ETAS to relate non-stationary seismicity rates to regional stress changes (Ogata, 1998, 2004, 2005). The difficulty with this approach is that it lacks a quantitative relationship between seismicity rate variations and stress/stressing-rate variations. However, it has been used to resolve time dependence of the background triggering rate by binning unusually large earthquake swarms into smaller (moving window) time periods that are assumed to have a stationary background rate within the time window (Hainzl and Ogata, 2005).

An alternative approach that is being utilized to map seismicity rate variations directly into stressing rate variations is a physical model based on rate- and state-dependent friction (Dieterich, 1994; Dieterich et al., 2000). This model incorporates several properties of laboratory friction measurements including an Omori-like response to a step change in stress-level. It has had several successful applications including retrieving the magnitude of stress steps using laboratory derived friction parameters (Dieterich et al., 2000) and predicting the spatial distribution of seismicity rate changes and aftershock sequence durations based on a geodetically derived model of stressing rate transients (Toda et al., 2002). However, both these applications occurred in volcanic regions where aftershock sequences are often subdued due to high geothermal gradients (Kisslinger and Jones, 1991; Ben-Zion and Lyakhovsky, 2006). In contrast, Toda and Matsumura (2006) used this method to estimate spatio-temporal stress changes from seismicity rate changes during a M_w 7.0 slow subduction zone earthquake in Tokai, Japan. Despite the extremely large magnitude of the slow event, the stressing rate changes retrieved by the rate–state inversion were not clearly distinguishable from other variations in the area. Some of this lack of resolution likely results from the contamination of moderate aftershock sequences in the stress vs. time curves produced by the rate–state inversion algorithm.

We seek to combine the strengths of the ETAS and rate–state approaches to develop an effective tool to detect anomalous seismicity rates and relate them to changes in stressing rates caused by physical processes. There have been recent attempts to combine the two models of seismicity rate for different purposes. For example, Console et al. (2006, 2007) combine the two models in order to produce a new model of earthquake clustering that incorporates physical constraints with a minimum number of free parameters. However, a combined ETAS/rate–state model that can be used in a single algorithm to detect anomalous stressing rates from seismicity rates has not been developed yet. Ogata (2005) demonstrated that even small changes in stress can cause anomalies in seismicity rate, and so a combined ETAS/rate–state model of seismicity rate has the potential to be a highly sensitive detector of transient deformation.

To develop such a combined model of seismicity rate, we first identify parameters that are related between the two models and examine their dependence on stressing rate. To clarify the stressing rate dependence of the aftershock parameters, we analyze data from 4 different earthquake swarms in various tectonic settings. We then specify a functional form for the seismicity rate in a combined ETAS/rate–state model, in which aseismically-triggered and coseismically-triggered components of seismicity rate are independent of one another. This suggests that an aseismically-triggered seismicity rate can be isolated from a catalog and used to directly estimate stressing rate changes associated with transient deformation.

2. Models

In general, the seismicity rate R in a catalog is a function of the stressing rate $\dot{S}$ acting on a fault (Dieterich, 1994). Earthquake catalogs contain seismicity triggered by different underlying mechanisms, such as earthquake–earthquake interactions, aseismic deformation, or background plate tectonic motion. Therefore, in our model, we consider three primary contributions to R:

$$R(x,t) = f(\dot{S}) = f(R_A, R_C, R_T)$$

where R_A represents the seismicity rate triggered by aseismic processes such as slow slip or dike intrusion, R_C reflects seismicity triggered by other earthquakes (e.g., aftershock sequences), and R_T is triggered by long-term tectonic loading. Because the tectonic component R_T is presumably small if aseismic processes are occurring, we simply combine it with R_A, so that $R(x,t) \approx f(R_A, R_C)$.

In order to develop a model that can quantitatively relate stressing rates to seismicity rates, we need to know the stressing rate dependence of each of the components of R. Toda et al. (2002) and Lohman and McGuire (2007) showed that seismicity rates clearly increase during periods of increased stressing rate caused by aseismic processes. Both studies found that the increase in earthquake rate was approximately equal to the increase in stressing rate so R_A likely scales linearly with stressing rate as predicted by the rate–state model.

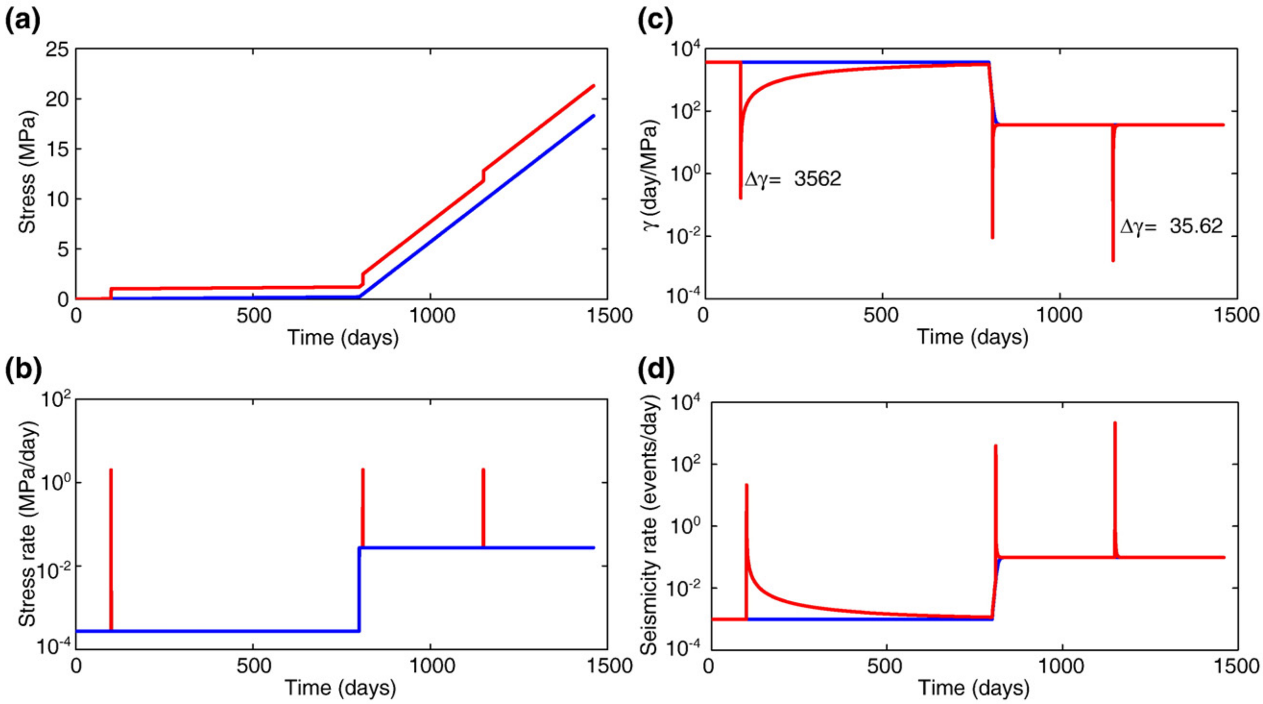

Fig. 1. Calculation of seismicity rates using forward simulation of rate–state model equations for two different stress histories, with $A\sigma = 0.1$ MPa. a) Stress histories for two cases: i) increase in stressing rate by 2 orders of magnitude (blue), and ii) increase in stressing rate by 2 orders of magnitude plus sudden stress changes (earthquakes) (red). b) Stressing rate histories for both cases. c) Evolution of γ from using Eqs. (3) and (4). d) Seismicity rate estimates obtained from stressing rates using Eq. (2).

The stressing rate dependence of R_C is less certain. The two main approaches to modeling the change in seismicity rate following an earthquake (i.e., R_C) are the stochastic Epidemic Type Aftershock Sequence (ETAS) model (Ogata, 1988), which is based on Omori's law (Omori, 1894), and the physically based rate–state friction model, which reproduces Omori's law following a sudden stress change (Dieterich, 1994). In this section we summarize the two models and compare how they predict R_C changes with stressing rate.

2.1. ETAS model

The ETAS model is a point process model that generalizes the modified Omori law (Omori, 1894; Utsu, 1961; Ogata, 1988). In this model, every aftershock has some probability of generating its own aftershocks. Therefore, the seismicity rate at some time t can be obtained by summing the aftershock sequences produced by each event that has occurred prior to time t plus a background seismicity rate μ:

$$R(t) = \mu + \sum_{t_i \le t} \frac{Ke^{\alpha(M_i - M_c)}}{(t - t_i + c)^p} \tag{1}$$

where c and p are the Omori decay parameters, α is related to the efficiency of an earthquake of a given magnitude at generating aftershocks, and K reflects the aftershock productivity of a mainshock. These parameters are generally obtained using maximum likelihood estimation from the observed times t_i and magnitudes M_i of earthquakes in a catalog, given the magnitude of completeness M_c of the catalog (Ogata, 1988). The summation in Eq. (1) is essentially the coseismic component of seismicity rate (R_C), as it contains all the aftershock sequences in the catalog. Because the ETAS parameters are not explicitly related to stressing rate, R_C also is independent of stressing rate in the ETAS model.

2.2. Rate- and state-dependent friction model

In the rate–state model, the seismicity rate R for a given magnitude interval observed on a population of faults governed by rate- and state-dependent friction can be linked to a stressing rate $\dot{S}$ through the following equations that assume normal stress is constant (Dieterich, 1994):

$$R = \frac{r}{\gamma \dot{S}_r} \tag{2}$$

$$d\gamma = \frac{dt}{A\sigma}\left(1 - \gamma\dot{S}\right) \tag{3}$$

where r is the steady-state seismicity rate for the same magnitude interval associated with a reference stressing rate $\dot{S}_r$, S is a modified Coulomb stress function, γ is a state variable, and A is a fault constitutive parameter. We assume that the normal stress σ remains constant, and as a result treat $A\sigma$ as a constant frictional parameter and $\dot{S}$ as a shear stressing rate.

Using this formulation, given some knowledge of regional background seismicity and $A\sigma$, the stressing rate can be obtained from an observed seismicity rate simply by integrating Eqs. (2) and (3) (Dieterich et al., 2000). Fig. 1 illustrates the relationship between stressing rate and seismicity rate in the rate–state model. Given a stress history that involves a change in stressing rate by two orders of magnitude (Fig. 1a–b, blue), Eq. (3) can be used to calculate the related change in γ (Fig. 1c, blue), which can then be used in Eq. (2) to obtain the change in seismicity rate. Fig. 1d demonstrates that following a change in stressing rate by a factor of 100, a similar change in seismicity rate occurs after a time lag that is related to the parameter $A\sigma$.

Now consider a stress history that includes the same change in stressing rate as well as earthquakes (sudden stress steps) (Fig. 1a–b, red). Dieterich (1994) derived a solution for γ given a sudden stress change (Eq. B11 in the 1994 paper):

$$\gamma = \gamma_0 \exp\left[\frac{-\Delta S}{A\sigma}\right] \tag{4}$$

Using both Eqs. (3) and (4), the evolution of γ associated with this stress history can also be determined (Fig. 1c, red) and Eq. (2) used to obtain the seismicity rate (Fig. 1d, red).

This simple case shows that the rate–state model predicts that certain parameters describing aftershock decay change with stressing rate. For example, consider two of the sudden stress steps (earthquakes) shown in Fig. 1b, the first (at time $t=100$) which occurs prior to the stressing rate change and the third (at time $t=1150$) which occurs well after the stressing rate change. The seismicity rate following the first earthquake, which occurs during low stressing rates, takes longer to decay to the background rate than that following the second earthquake, which occurs during high stressing rates (Fig. 1d); thus, this characteristic relaxation time, t_a, depends on stressing rate as seen in the Miyake–Jima swarm (Toda et al., 2002).

This case also demonstrates that the change in seismicity rate immediately following the stress step also varies with stressing rate. Although the first and second earthquakes both had the same stress change, the peak seismicity rate is higher for the second earthquake than for the first. Because the change in seismicity rate ΔR due to the stress change depends on the change in γ, this is a direct consequence of Eq. (4). If we define $\Delta\gamma$ to be the change in γ due to the stress step (i.e., $\Delta\gamma=\gamma-\gamma_0$), it is easy to see from Eq. (4) that $\Delta\gamma$ will be a function of γ_0 (i.e., the value of γ prior to the stress step). Since the second earthquake occurs during the higher stressing rate, it has a lower γ_0, and therefore a smaller $\Delta\gamma$ and a larger ΔR than the first earthquake (Fig. 1c). Thus the seismicity rate immediately following a stress step depends on the stressing rate.

This prediction of the rate–state model can also be shown with a second simulation. Assuming a constant stressing rate following a stress step and steady-state seismicity rate prior to a stress step, Dieterich (1994) used Eqs. (2)–(4) to express the seismicity rate following a stress step as:

$$R(t) = \frac{r\frac{\dot{S}}{\dot{S}_r}}{\left[\frac{\dot{S}}{\dot{S}_r}\exp\left(\frac{-\Delta S}{A\sigma}\right)-1\right]\exp\left[\frac{-t}{t_a}\right]+1}, \quad \dot{S}\neq 0 \tag{5}$$

where

$$t_a = A\sigma / \dot{S} \tag{6}$$

is the characteristic relaxation time related to the time it takes for the seismicity rate to return to background levels. This takes the form of Omori's law for $t<t_a$.

Eq. (5) can be used to compare the seismicity rate change due to a uniform stress step during different magnitudes of stressing rate. Because Eq. (5) is only valid when the seismicity rate prior to the stress step is at steady-state, we assume that the reference seismicity rate r (i.e., the seismicity rate prior to the stress step) has already achieved a steady-state value at each of the stressing rate levels. Therefore, r will have a different value at each stressing rate (Fig. 2a, dashed lines), because as Eqs. (2) and (3) demonstrate, the steady-state seismicity rate scales with stressing rate (Fig. 1). Furthermore, we assume that the stressing rate before and after the stress step remains constant (i.e., $\dot{S}_r=\dot{S}$). Given these assumptions, we can use Eq. (5) to predict the seismicity rate R following a uniform stress step at different magnitudes of stressing rate relative to some background stressing rate $\dot{S}_b$, ranging from 1 to 1000 (Fig. 2a, solid lines). In agreement with the first simulation, the results show that as the stressing rate increases, the seismicity rate increases, while t_a decreases.

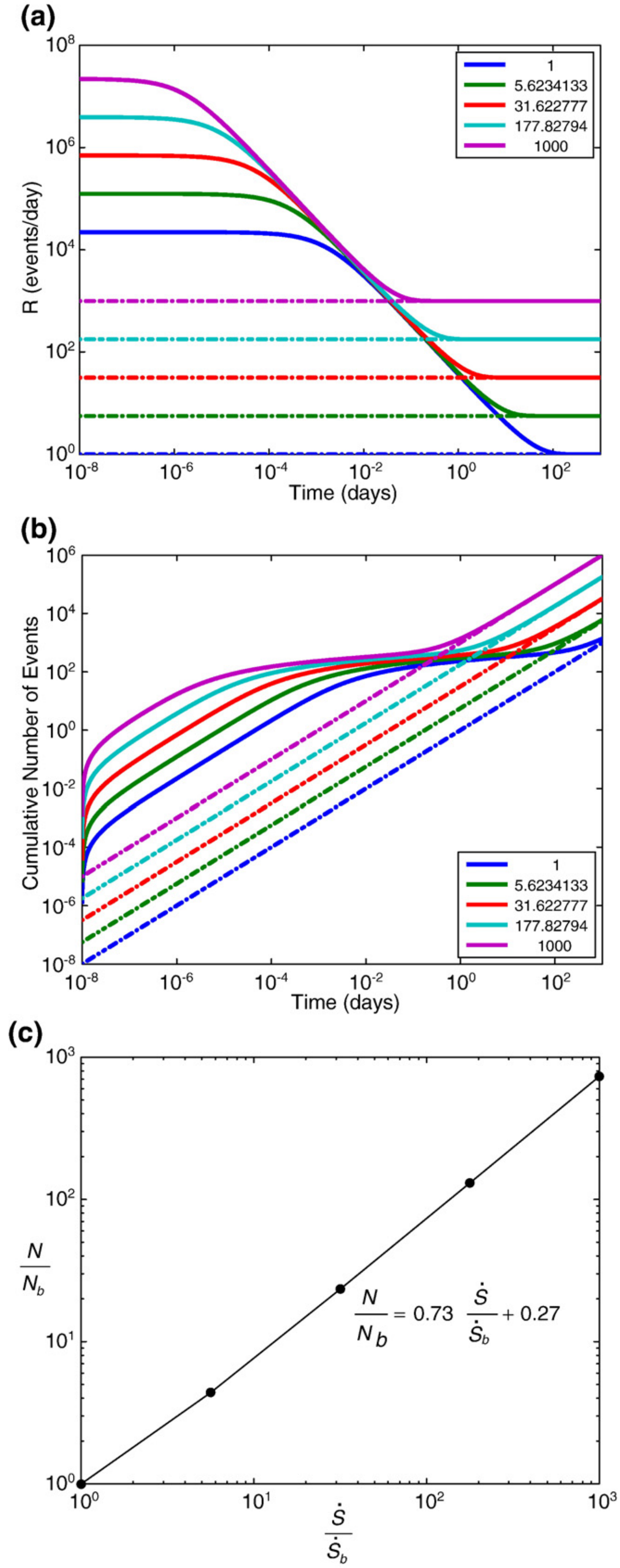

Fig. 2. a) Seismicity rate R calculated with Eq. (5) at different magnitudes of stressing rate $\dot{S}$ relative to a background stressing rate $\dot{S}_b=0.1$ MPa/yr (solid lines), using $\Delta S=0.1$ MPa and $A\sigma=0.01$ MPa. Colors indicate the stressing rate. Steady-state seismicity rate r for each stressing rate is also shown (dashed lines). As stressing rate increases, R increases while t_a decreases. b) Cumulative number of events over time obtained by integrating curves in Fig. 2a. The difference between solid and dashed lines of similar color represents aftershocks due to the sudden stress change that is present in the solid curves. c) Number of aftershocks N produced by the uniform stress change at each of the relative stressing rate values $\dot{S}/\dot{S}_b$, relative to number N_b produced at the background stressing rate. The least-squares fit shows that as stressing rate increases, the number of aftershocks also increases, indicating that the parameter K is dependent on stressing rate.

2.3. Combining the ETAS and rate–state models

To combine the ETAS and rate–state models into a single model appropriately, we now examine the relationships between parameters of both models and their dependence on stressing rate. The parameters we will consider are the ETAS parameters α, p, c, K, and μ. The dependence of these parameters on stressing rate will determine the dependence of R_C on stressing rate, which in turn will determine the functional form of R that we seek to establish.

The ETAS parameter α describes the efficiency of an earthquake of a given magnitude at generating aftershocks. It has no direct equivalent in the rate–state model, which incorporates no magnitude dependence in its equations. However, there is an implicit magnitude dependence in the rate–state model, in that larger earthquakes increase the stress-levels in a greater volume of the crust than small ones. Therefore, we assume that α is related to the spatial extent of a stress step and independent of stressing rate.

Simulations using Eq. (5) show that the ETAS parameter p is essentially 1 and independent of stressing rate in the rate–state model. Both theoretical and observational studies also suggest that this Omori decay parameter is more influenced by factors that are relatively stressing rate independent, such as heterogeneity in temperature/heat flow or structure (e.g., Mogi, 1962, 1967; Kisslinger and Jones, 1991; Utsu et al., 1995). Recently, Helmstetter and Shaw (2006) have also shown that p can be related to the rate–state parameter $A\sigma$ and the spatial distribution of the stress field on a fault. Therefore, as p seems to be more sensitive to longer-term heterogeneities on a fault, in our model we consider p independent of stressing rate.

In the rate–state model, the ETAS parameter c can be analytically related to rate–state parameters and stressing rate (Dieterich, 1994). In reality, it is difficult to obtain an accurate measurement of c because of the incomplete detection of early aftershocks (Utsu et al., 1995). Therefore, any dependence that c may have on stressing rate will most likely be obscured by this effect, and so we consider c independent of stressing rate.

The last two ETAS parameters (K and μ) do not have as straightforward a relationship with stressing rate. The rate–state model predicts that background seismicity rate (i.e., seismicity not triggered by an earthquake) depends on stressing rate. As the stressing rate increases, so does the background seismicity rate (blue lines in Fig. 1, dashed lines in Fig. 2). The ETAS model on the other hand assumes that background seismicity rate μ is constant in a particular time interval.

The ETAS model also assumes that aftershock productivity K is independent of stressing rate. On the other hand, the rate–state model predicts that K increases with stressing rate. Therefore, an earthquake with a given stress drop that occurs during a time of lower stressing rate will produce fewer aftershocks than if it had occurred during a time of higher stressing rate.

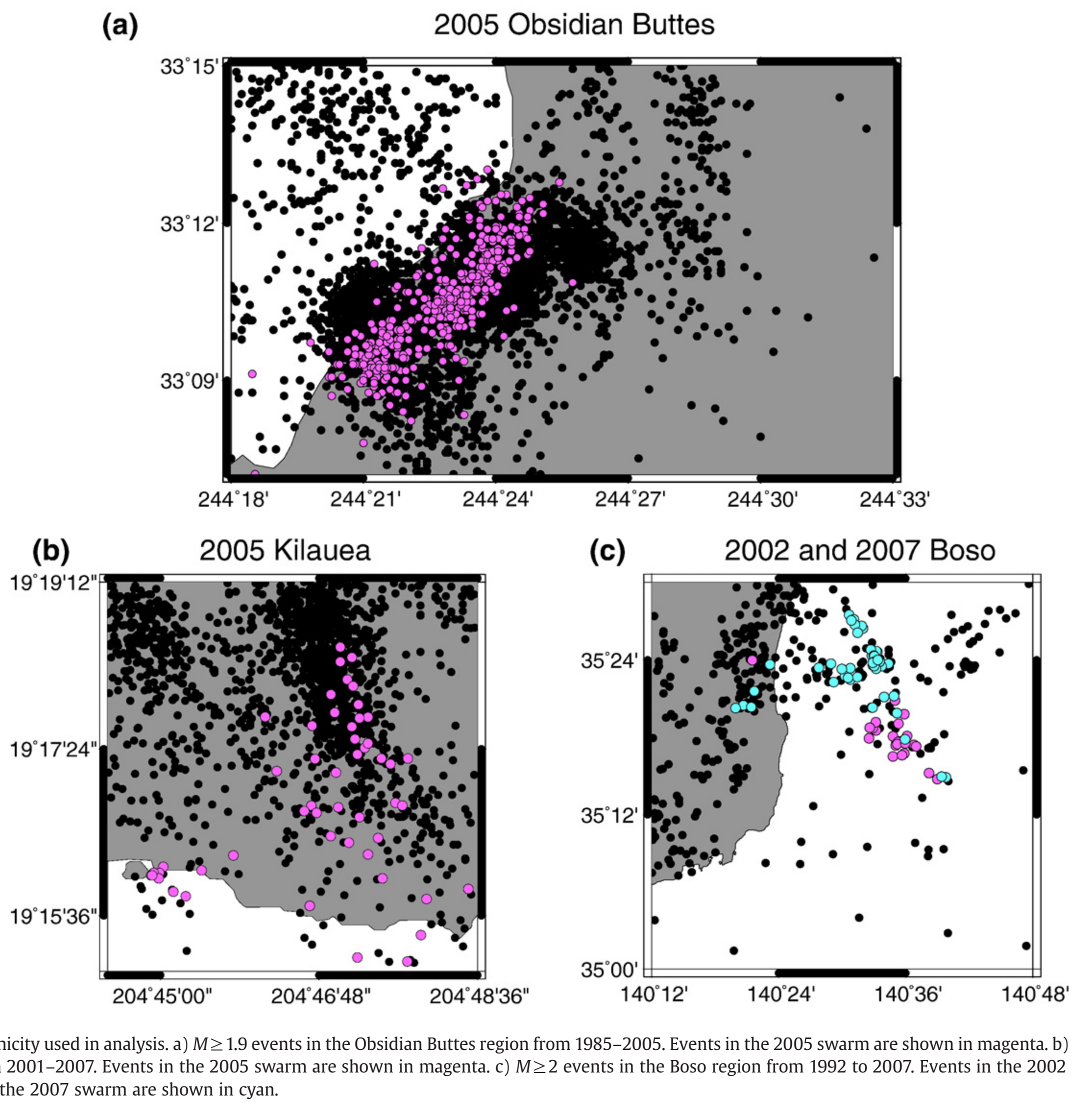

Fig. 3. Maps of seismicity used in analysis. a) $M \geq 1.9$ events in the Obsidian Buttes region from 1985–2005. Events in the 2005 swarm are shown in magenta. b) $M \geq 1.5$ events in the Kilauea region from 2001–2007. Events in the 2005 swarm are shown in magenta. c) $M \geq 2$ events in the Boso region from 1992 to 2007. Events in the 2002 swarm are shown in magenta, events in the 2007 swarm are shown in cyan.

The simulations using Eq. (5) demonstrate this behavior. The seismicity rates associated with the five different stressing rates in Fig. 2a are integrated to determine the cumulative number of events for each stressing rate (Fig. 2b). When comparing the case with a stress step (solid lines) to the case with no stress step (dashed lines), the difference between the two curves at a given stressing rate is due to the aftershocks produced by the stress step. We can then compare the number of aftershocks N produced by uniform stress changes at the five different stressing rates to the number of aftershocks N_b produced by the same stress change at the background stressing rate (Fig. 2c). As the stressing rate increases, the number of aftershocks produced also increases. For example, an earthquake that occurs at a stressing rate 1000 times higher than the background stressing rate produces ~700 times more aftershocks than a similar sized earthquake occurring at the background stressing rate when $A\sigma = 0.01$ MPa. The ratio N/N_b thus reflects the increase in aftershock productivity K predicted by the rate–state model due to the increase in stressing rate unlike the ETAS model, in which K is not related to stressing rate. Therefore, the main issues that need to be resolved in order to build a consistent combined model of seismicity rate involves ascertaining the dependence of K and background seismicity rate μ on stressing rate.

3. Data analysis

Many studies suggest that swarms are a response to geodetically observed increases in stressing rate (e.g., Lohman and McGuire, 2007; Ozawa et al., 2007). Therefore, by analyzing swarms, we can establish whether the ETAS parameters K and μ change during periods of high stressing rates. We use three types of analyses: first, we fit the ETAS model to a catalog containing a swarm to determine if the triggering behavior is non-stationary during swarms. Second, we divide the catalog into pre-swarm and swarm portions, fit the ETAS model to each and compare the parameter estimates to determine how they change during swarms. Finally, we compare aftershock counts of a moderate-sized earthquake that occurred during a stressing rate transient to aftershock counts of other earthquakes in the catalog to test the rate–state model prediction that aftershock productivity K scales with stressing rate.

We examine 4 earthquake swarms that geodetic studies have linked to changes in stressing rate: the 2005 Obsidian Buttes swarm (Lohman and McGuire, 2007), the 2005 Kilauea swarm (Wolfe et al., 2007), and the 2002 and 2007 Boso swarms (Ozawa et al., 2003, 2007). Catalogs for these swarms were obtained from the Southern California Earthquake Data Center, the Advanced National Seismic System, and the Japan Meteorological Agency respectively.

3.1. Detection of anomalous seismicity rates

The ETAS model when used as a diagnostic tool can identify time periods when seismicity rates do not behave as typical aftershock sequences (Ogata, 1988; McGuire et al., 2005). We apply the method described in Ogata (2005) by fitting the ETAS model to a catalog that includes a swarm. We then employ a transformation described in Ogata (1988) which utilizes the following theoretical cumulative function:

$$\Lambda(t) = \int_0^t R(s)\mathrm{d}s \tag{7}$$

where R is the seismicity rate predicted by the ETAS model (Eq. (1)). The occurrence times t_i in the catalog are transformed into $\tau_i = \Lambda(t_i)$. If the earthquakes in the catalog are described well by the ETAS model, then t_i will be distributed according to a stationary Poisson process, and a plot of the actual cumulative number of events vs. the theoretical number of events (i.e., the transformed time τ) will be linear. Anomalous seismicity that the ETAS model cannot explain will appear as deviations from this trend.

3.1.1. 2005 Obsidian Buttes swarm

In August 2005, an earthquake swarm occurred over the course of two weeks on a continental strike-slip fault in the Salton Trough in

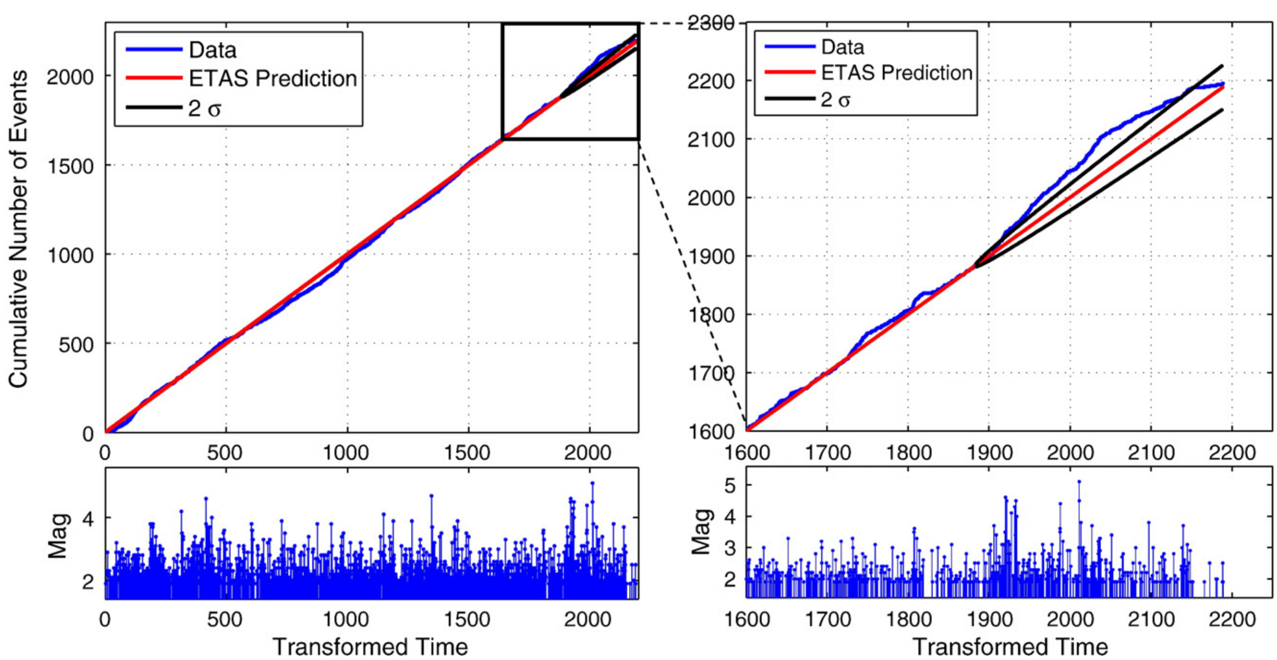

Fig. 4. Results of optimization of the ETAS model for the 2005 Obsidian Buttes catalog, comparing the cumulative number of events to the transformed time (ETAS predicted number of events). The observed data are shown in blue and the ETAS prediction in red. Bottom panels show the magnitudes of the events in the swarm. The ETAS model is optimized until just prior to the swarm and extrapolated for the remainder of the catalog. Black lines signify the 2σ bounds of the extrapolation. A significant deviation from the ETAS prediction occurs near the beginning of the swarm. (for interpretation of the references to colour in this figure legend, the reader is referred to the web version of this article.)

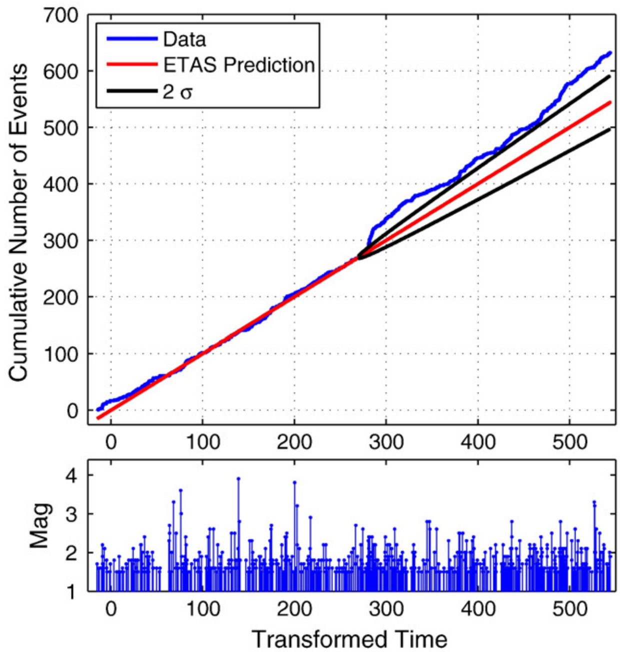

Fig. 5. Results of ETAS model optimization for the 2005 Kilauea catalog. See Fig. 4 for symbol explanation. The ETAS model ceases to adequately fit the catalog early in the swarm.

southern California. Lohman and McGuire (2007) concluded that the swarm was triggered primarily by aseismic fault creep that released moment equivalent to a M_w 5.7 earthquake and increased the stressing rate (and seismicity rate) by about a factor of 1000.

The earthquake catalog used in our analysis consists of events from 1985–2005, with a magnitude of completeness $M_c = 1.9$ (Fig. 3a). The ETAS model was optimized through 2005 until just prior to the swarm and then extrapolated until 2006. The transformed time plot shows that a significant deviation from the ETAS predicted trend occurs at the time of the swarm (Fig. 4). More events occurred during the swarm than the ETAS model can explain with the parameters that best fit the preceding catalog. This suggests that at least one of the ETAS parameters changes during periods of high stressing rate.

3.1.2. 2005 Kilauea swarm

Slow earthquakes that trigger microseismicity periodically occur on the south flank of Kilauea Volcano in Hawaii (Cervelli et al., 2002; Brooks et al., 2006; Segall et al., 2006; Wolfe et al., 2007). In this study, we focus on a slow earthquake that occurred on 26 January 2005 and released moment equivalent to a M_w 5.8 earthquake over the course of hours to days (Brooks et al., 2006; Wolfe et al., 2007).

The catalog we analyze consists of events occurring from 2001–2007, with a catalog completeness of $M_c = 1.5$ (Fig. 3b). We optimize the ETAS model from 2001–2005 and extrapolate through the remainder of the catalog. Again, the results show that a significant deviation from typical aftershock behavior occurs at the time of the swarm (blue curve above the black confidence limits in Fig. 5), suggesting a stressing rate dependence of one or more parameters.

3.1.3. 2002 and 2007 Boso swarms

The Boso peninsula in central Japan has been the site of recurring slow slip events on the subduction thrust interface in 1996, 2002 and 2007 (Ozawa et al., 2003; Sagiya, 2004; Ozawa et al., 2007). These events, detected by GPS instruments, lasted on the order of a week and were accompanied by earthquake swarm activity. Ozawa et al. (2007) suggest that the slow slip events are the primary driving process

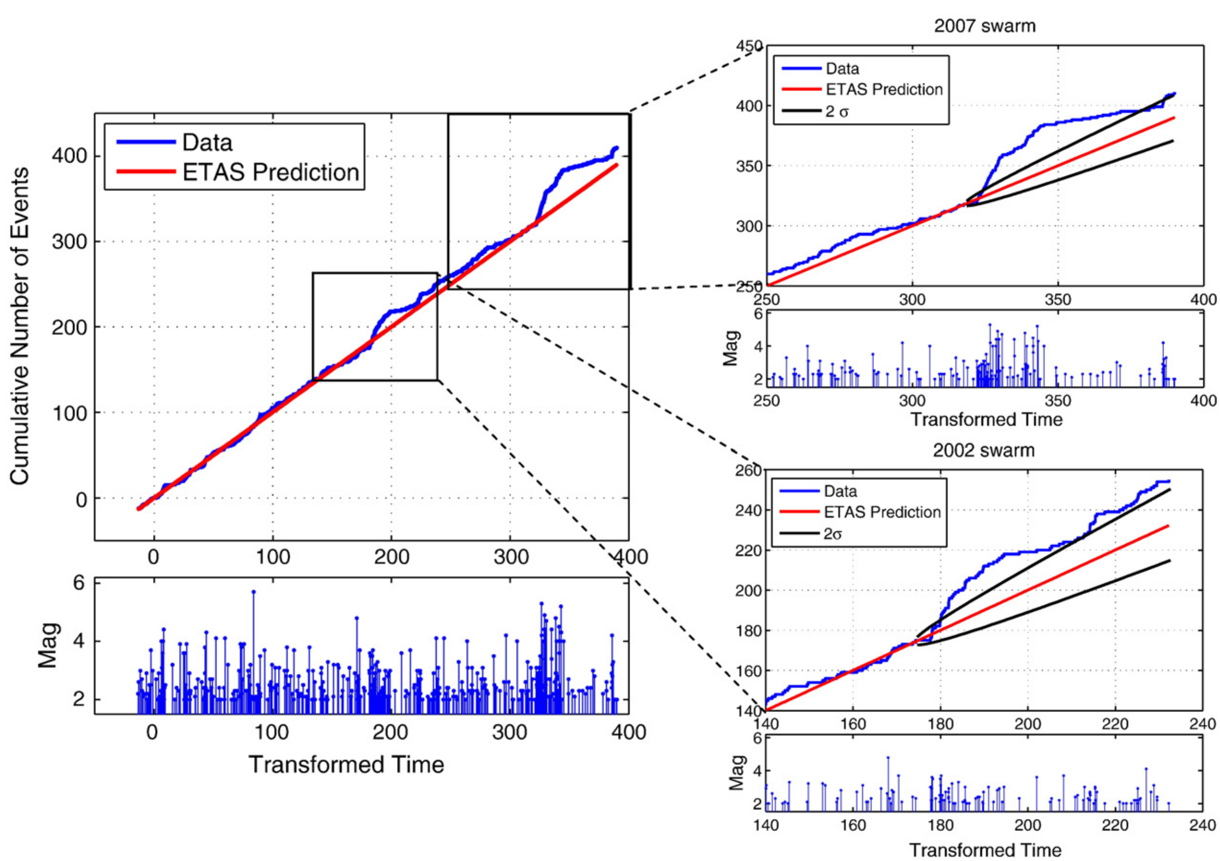

Fig. 6. Results of ETAS model optimization for the 2002 and 2007 Boso swarms. See Fig. 4 for symbol explanation. For both swarms, the ETAS model again fails to explain the amount of seismicity that occurs during the swarms, indicating that the ETAS parameters that best fit the catalog prior to the swarms no longer fit during the swarms.

Table 1
Comparison of maximum likelihood estimates of ETAS parameters before and during each swarm.

Swarm	Pre-swarm MLE (K, μ, α, p, c)	Swarm MLE (K, μ, α, p, c)
2002 Boso	0.13, 0.022, 0.56, 1.11, 0.096	0.07, 2.09, 0.09, 1.0, 0.0005
2005 Kilauea	0.28, 0.16, 1.24, 1.21, 0.002	0.96, 0.89, 0.61, 0.92, 0.003
2005 Obsidian Buttes	0.61, 0.031, 0.88, 1.1, 0.001	1.4, 225, 1.05, 1.0, 0.001
2007 Boso	0.20, 0.013, 0.55, 0.88, 0.0004	0.61, 2.4, 1.37, 1.0, 0.0008

triggering the swarms, similar to the Obsidian Buttes swarm (Lohman and McGuire, 2007).

Our catalog consists of $M \geq 2$ events from 1992 to 2007 (Fig. 3c). To obtain the best-fitting parameter estimates for the catalog as a whole, the ETAS model is optimized from 1992 to February 2007 and extrapolated through 2008. Due to the short duration of the 2002 swarm, it should have very little effect on the parameter estimates. The results indicate that anomalous seismicity rates occur during the slow slip events in 2002 and 2007 that cannot be explained by the ETAS model (Fig. 6). Again, this suggests that at least one ETAS parameter depends on stressing rate.

3.2. Fitting ETAS to earthquake swarms

One way to determine which ETAS parameters change during swarms (i.e., high stressing rate periods) is to fit the ETAS model to the pre-swarm portion of the catalog and compare it to ETAS fit to the swarm alone. Table 1 shows the pre-swarm and swarm estimates of

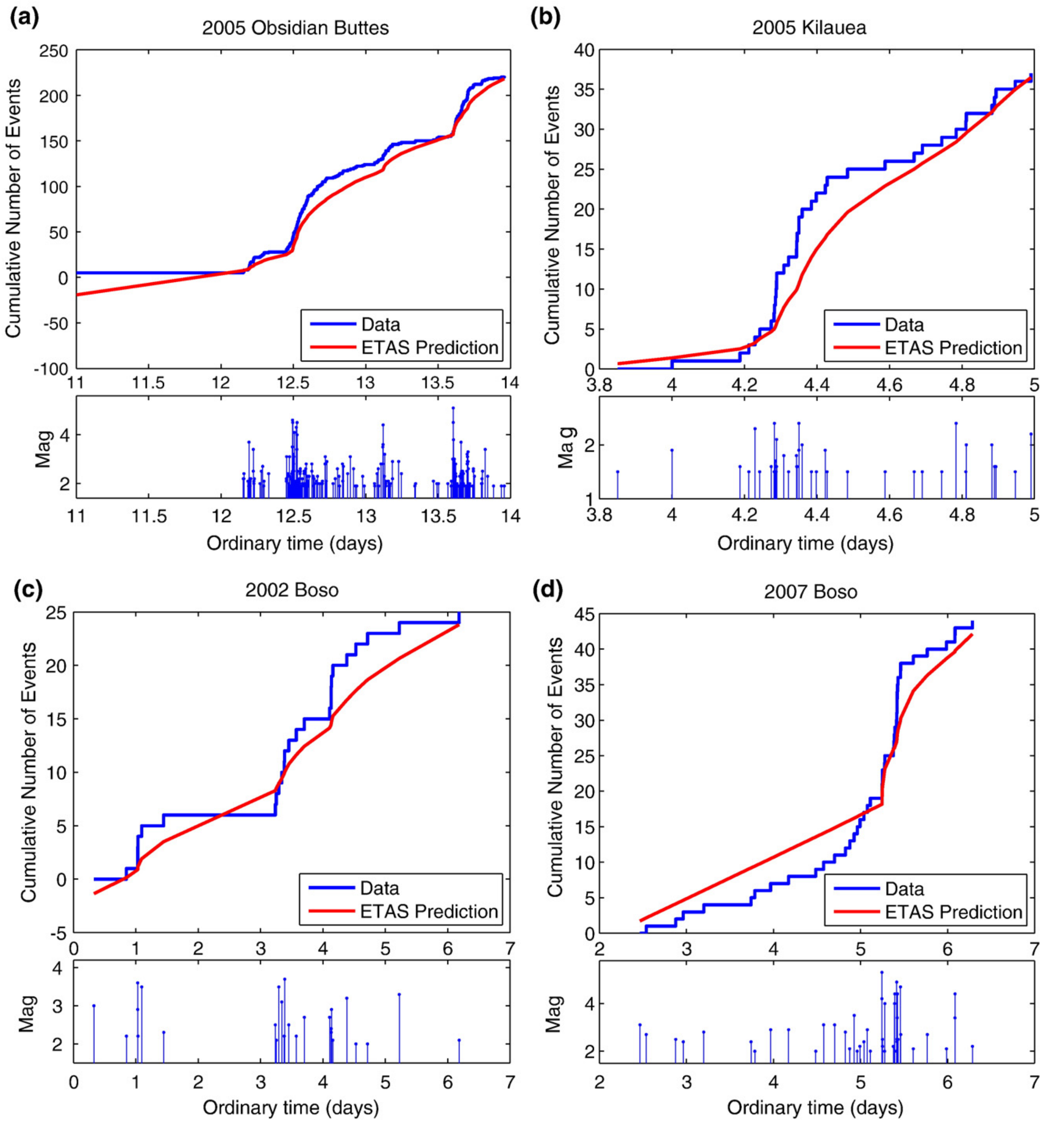

Fig. 7. Results of applying the ETAS model only on swarm seismicity from a) the 2005 Obsidian Buttes catalog, b) the 2005 Kilauea catalog, c) the 2002 Boso catalog, and d) the 2007 Boso catalog. In all 4 cases, the ETAS model requires increases in K and μ compared to pre-swarm estimates in order to adequately fit the data during the swarm.

the ETAS parameters for each swarm. In most cases, in order for the model to converge, p was held fixed at 1.0. The observed and predicted cumulative numbers of events for each swarm are shown in Fig. 7a–d. The poorer quality of the fits could suggest that a time-dependent μ may be necessary to more accurately fit the data. For all of the swarms, the ETAS model finds changes in K by factors of 2–4. However, the parameter μ increases by 1–3 orders of magnitude during the swarms. Therefore, with the ETAS model, stressing rate transients appear to primarily increase the background seismicity rate without increasing aftershock productivity substantially.

3.3. Comparison of rate–state predictions with observations

A final way to test the stressing rate dependence of K is to look at moderate sized earthquakes that occur during a swarm. By counting the number of aftershocks following these earthquakes (in narrow space–time windows) and comparing to the number of aftershocks produced by other earthquakes in the catalog (during low stressing rate periods), we can test the hypothesis that K is stressing rate dependent. Assuming that the ETAS parameters α, p, and c remain constant over time, the average number of aftershocks following an earthquake of magnitude M can be expressed as:

$$N = \frac{K}{1-n} 10^{\alpha(M-M_c)} \tag{8}$$

where the branching ratio $n = Kb/(b-\alpha)$ (Helmstetter and Sornette, 2003; McGuire et al., 2005). Therefore, if the ETAS and Gutenberg–Richter parameters are assumed to remain constant throughout the catalog, N is primarily a function of the difference between mainshock magnitude M and catalog completeness threshold M_c, and a plot of the logarithm of aftershock counts of mainshocks in the catalog will be linear with respect to the mainshock magnitudes (McGuire et al., 2005). In contrast, the rate–state equations predict a greater productivity (larger K) during the transient and Eq. (8) will not describe the data well.

Fig. 8 shows the aftershock productivity for the Obsidian Buttes catalog. Aftershocks in a 1-day time window were counted for mainshocks with $M \geq 4$, occurring sufficiently apart in time so as not to interact with one another. During the swarm, Lohman and McGuire (2007) estimated that a stressing rate transient of ~1000 times the background stressing rate occurred. Therefore, the rate–state model equations predict that the M5.1 earthquake that occurred during the swarm should produce almost 1000 times more aftershocks than a similar sized earthquake occurring at typical stressing rates (Fig. 2c). However, the actual number of aftershocks observed following the earthquake was not that large (star in Fig. 8). The aftershock count for this event in fact plots on the same constant line as the other events in the catalog, suggesting that K is independent of stressing rate. A concern is that the lack of increase in K could be due to the incomplete detection of early aftershocks. However, we have carefully taken the magnitude of completeness M_c into account for each of the catalogs in our analysis. Moreover, the rate–state model equations and thus predictions are defined for a given magnitude interval that we assume to be $M \geq M_c$ (Dieterich, 1994). Therefore, undetected aftershocks are unlikely to be the primary reason for the lack of an increase in K.

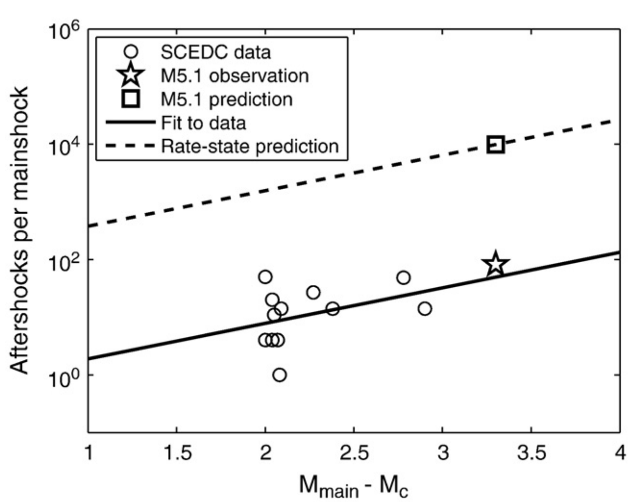

Fig. 8. Aftershocks per mainshock vs. difference between mainshock magnitude and magnitude of completeness $M_c = 1.9$ for events of $M_{main} \geq 4$ in the Obsidian Buttes catalog from 1985–2005 (circles). Aftershocks for each event were counted within a 1 day window. Lines depict lines of constant aftershock parameters, where number of aftershocks depends on $M_{main} - M_c$. Solid line shows least-squares fit to data; dashed line shows increase in aftershock productivity predicted by rate–state model for a stressing rate of 1000 times background stressing rate. The actual number of aftershocks following the M5.1 mainshock (star) is much less than the number predicted by the rate–state model (square) and falls on a line consistent with other mainshocks in the catalog, suggesting that K (i.e., aftershock productivity) is not stressing rate dependent.

3.4. Summary

We have analyzed 4 different earthquake swarms to examine the dependence of the ETAS parameters K and μ on stressing rate. The ETAS model identified the swarms as anomalous seismicity that cannot be fit with the same parameters as the rest of the catalog, suggesting that at least one of the parameters changes with stressing rate. However, when the ETAS model was fit to the swarms alone, estimates for K changed very little compared to the pre-swarm fit while the estimates for μ increased by several orders of magnitude. Finally, the aftershock count following the M5.1 Obsidian Buttes earthquake revealed no substantial increase in K during the heightened stressing rate associated with the swarm. Together these results suggest that stressing rate transients increase the background seismicity rate μ without causing a substantial increase in aftershock productivity K.

4. Discussion and conclusion

The primary conflict between the ETAS and rate–state models of seismicity rate lies in the dependence of aftershock productivity on stressing rate. Our results suggest that, contrary to rate–state model predictions, the aftershock productivity is unaffected during stressing rate transients, which instead increase the background seismicity rate. The key to this discrepancy lies in the evolution of the rate–state variable γ. In the rate–state model, an increase in seismicity rate implies that γ has evolved to a new steady-state value (Eq. (2)). Our simulations show that with this increase in seismicity rate comes an increase in aftershock productivity (Fig. 2). Therefore, the lack of an increase in productivity suggests that the state variable γ has not evolved. Thus, there is a fundamental conflict between the heightened seismicity rate and the unchanged aftershock productivity we have observed in our analysis of swarms.

An additional complication is that the evolution of γ also depends on the frictional parameter $A\sigma$ (see Eq. (3)). This parameter controls how quickly γ evolves in response to changes in stressing rate, and therefore ultimately affects the aftershock productivity of a stress step. We can again use Eqs. (2)–(4) to explore in detail how the change in aftershock productivity with stressing rate varies with $A\sigma$. We compare two stress histories, one in which an earthquake ($\Delta S = 1$ MPa) occurs during a background stressing rate of 0.2 MPa/yr, and one in which a similar stress step occurs three days after a stressing rate transient begins. We use Eqs. (3) and (4) to calculate γ for each stress history and Eq. (2) to obtain seismicity rates that can then be integrated to estimate the number of aftershocks produced by each earthquake. Fig. 9 compares the number of aftershocks N_2 produced by an earthquake that occurs three days after a stressing rate

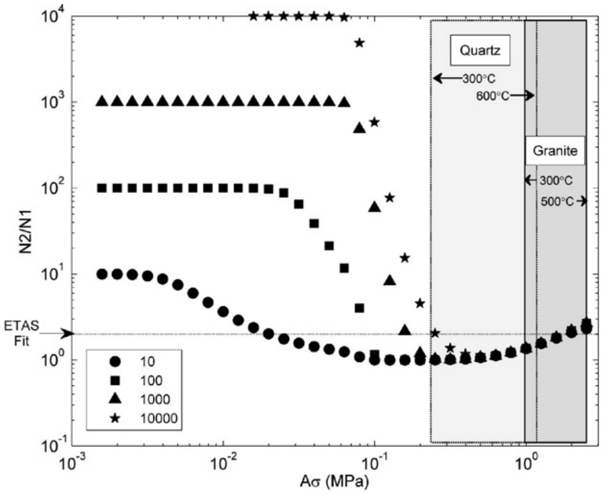

Fig. 9. Change in aftershock productivity N_2/N_1 vs. $A\sigma$ following various magnitudes of stressing rate jumps relative to the background stressing rate of 0.2 MPa/yr (symbols), for an earthquake with $\Delta S = 1$ MPa. The ratio predicted by the ETAS fits in Table 1 for the Obsidian Buttes swarm is indicated. Values for $A\sigma$ are also shown, given laboratory values of A for quartz (Chester and Higgs, 1992) and granite (Blanpied et al., 1998) in hydrostatic conditions at a depth of 4 km for temperatures ranging from 300 °C to 600 °C. For any given range of $A\sigma$, the rate–state model cannot satisfy both the increase in seismicity/stressing rate and the lack of change in aftershock productivity observed during the Obsidian Buttes swarm.

transient begins to the number of aftershocks N_1 produced by an earthquake that occurs during the background stressing rate, using different values of $A\sigma$ ranging from 10^{-3} to 3 MPa. The ratio N_2/N_1 essentially gives the expected increase in aftershock productivity K during a stressing rate transient. Fig. 9 demonstrates that the predicted change in aftershock productivity is highly dependent on the value of $A\sigma$ used in the rate–state equations.

Catalli et al. (2008) recently examined the role of $A\sigma$ in modeling seismicity rate variations and found that it controlled the total number of aftershocks triggered by an earthquake primarily in two ways. First, $A\sigma$ controls the instantaneous change in γ (and therefore seismicity rate) due to a sudden stress step (Eq. (4)), so that as $A\sigma$ increases, the instantaneous change in seismicity rate decreases. Second, the duration of aftershock sequences, t_a, also depends on $A\sigma$; as $A\sigma$ increases, t_a increases (Eq. (6)). The simulations in this study demonstrate that these two effects are also dependent on stressing rate (Figs. 1–2). As stressing rate increases, the change in seismicity rate due to a stress step increases, but the aftershock duration t_a decreases. Therefore, the range of aftershock productivity behavior seen in Fig. 9 reflects the tradeoffs in how these two effects are controlled by both $A\sigma$ and stressing rate.

To compare this predicted behavior with a real-life example, for the 2005 Obsidian Buttes M5.1 earthquake, which occurred three days after an increase in stressing rate of almost three orders of magnitude, we found $N_2/N_1 \sim 1$ from aftershock counts (Fig. 8). Additionally, the ETAS model fitting resulted in an increase in background seismicity rate by over three orders of magnitude (Table 1), which agrees with the observed increase in seismicity rate. Fig. 9 shows that the rate–state model cannot satisfy all of these observations in a small range of $A\sigma$. Typical estimates of $A\sigma$ from earthquake catalogs range from 10^{-3} to 10^{-1} MPa (e. g., Gross and Kisslinger, 1997; Harris and Simpson, 1998; Toda et al., 1998; Belardinelli et al., 1999; Console et al., 2007). In this range of $A\sigma$, γ evolves quickly, so that jumps in stressing rate cause jumps in seismicity rate, but also cause jumps in N_2/N_1 (i.e., aftershock productivity). Laboratory measurements of A for quartz and granite (Chester and Higgs, 1992; Blanpied et al., 1998) result in higher values of $A\sigma$ (10^{-1} to 1 MPa) for faults under hydrostatic pore pressure at a depth of 4 km. At these values of $A\sigma$, although aftershock productivity does not change with the jump in stressing rate, neither does the seismicity rate, because γ has not evolved to any great extent. We find that the increase in seismicity rate and the lack of change in aftershock productivity observed in the Obsidian Buttes swarm cannot both be satisfied simultaneously using the rate–state model, because the two observations imply fundamentally different things about whether γ has evolved or not. Therefore, some caution is necessary when applying the rate–state inversion algorithm to obtain stressing-rate changes from earthquake catalogs.

Given our observations of the dependence of the ETAS parameters on stressing rate, we can now specify a combined ETAS/rate–state model of seismicity rate to detect stressing rate transients from earthquake catalogs. As described earlier, the seismicity rate R in a catalog is a function of an aseismically-triggered component R_A and an earthquake–earthquake triggered component R_C. While R_A is clearly related to stressing rate, the relationship between R_C and stressing rate was unclear. Our results suggest that K is independent of stressing rate for a particular region, and so R_C is independent of stressing rate. R can then essentially be separated into the aseismic component R_A and the coseismic component R_C (represented by the ETAS model):

$$R = R_A + R_C = R_A + \sum_{t_i \le t} \frac{K e^{\alpha(M_i - M_c)}}{(t - t_i + c)^p} \tag{9}$$

Then R_A is effectively a time dependent version of the ETAS parameter μ (see Eq. (1)), and to obtain it, one can simply subtract the ETAS-predicted R_C from the observed rate R. The residual R_A can then be directly related to a stressing rate $\dot{S}_A$ caused by aseismic deformation through the rate–state model equations:

$$R_A = R - R_C = R - \sum_{t_i \le t} \frac{K e^{\alpha(M_i - M_c)}}{(t - t_i + c)^p} = \frac{r}{\dot{S}_r \gamma} \tag{10}$$

$$d\gamma = \frac{dt}{A\sigma}\left[1 - \gamma\left(\dot{S}_A + \dot{S}_b\right)\right] \tag{11}$$

where $\dot{S}_b$ is the background tectonic stressing rate. The use of the ETAS model to estimate R_C reduces the impact of aftershock sequences on the estimation of the aseismically-triggered seismicity rate, while the rate–state model establishes the relationship between aseismically-triggered seismicity rates and stressing rates.

There are a number of caveats to keep in mind about this model. First, a fundamental assumption this model makes is that the ETAS parameters K, α, c and p are constant in space and time and can describe all coseismically-triggered seismicity in a catalog completely. These parameters can in fact vary from sequence to sequence, as well as place to place (Ogata, 1998). However, our data analysis suggests that at least within relatively small and homogeneous regions, these parameters will remain constant, and therefore changes in the observed seismicity rate will be primarily mapped into changes in R_A. Second, practical applications of this model will have to be careful about catalog completeness, to ensure that undetected events such as early aftershocks do not affect the results. An additional point to bear in mind is the need to smooth the seismicity rates over some time window. Currently there is no way to estimate R_A at arbitrarily fine time scales, so algorithms will need to be developed to smooth these estimates in an optimal way. These issues will need to be considered when this model is implemented in an algorithm to invert for stressing rate variations, but the studies of Toda et al. (2002) and Lohman and McGuire (2007) suggest that our model is correct at least at the order of magnitude level. To verify the rate–state equations for background rate at a higher level of precision would require high sample-rate geodetic measurements (e.g., strain- or tiltmeters). However, to first order, our model provides a simple and direct way to quantitatively relate aseismic stressing rate transients to seismicity data and will allow future studies to invert seismicity catalogs to detect stressing rate variations caused by transient aseismic processes.

Acknowledgments

We thank R. Stein, S. Toda, and J. Dieterich for helpful discussions that increased our understanding of the rate–state model, and three anonymous reviewers whose comments improved the paper. Earthquake catalogs were obtained from the Advanced National Seismic System, Japan Meteorological Agency, and the Southern California Earthquake Data Center. Map figures were prepared using the Generic Mapping Tools software freely distributed by Wessel and Smith (1998). This work was supported by NSF EAR grant #0738641 (McGuire and Llenos) and a National Defense Science and Engineering Graduate Fellowship (Llenos).

References

Audigane, P., Royer, J.J., Kaieda, H., 2002. Permeability characterization of the Soultz and Ogachi large-scale reservoir using induced microseismicity. Geophysics 67, 204–211. doi:10.1190/1.1451573.

Belardinelli, M.E., Cocco, M., Coutant, O., Cotton, F., 1999. Redistribution of dynamic stress during coseismic ruptures: evidence for fault interaction and earthquake triggering. J. Geophys. Res. 104, 14925–14945.

Ben-Zion, Y., Lyakhovsky, V., 2006. Analysis of aftershocks in a lithospheric model with seismogenic zone governed by damage rheology. Geophys. J. Int. 165, 197–210. doi:10.1111/j.1365-246X.2006.02878.x.

Blanpied, M.L., Marone, C.J., Lockner, D.A., Byerlee, J.D., King, D.P., 1998. Quantitative measure of the variation in fault rheology due to fluid–rock interactions. J. Geophys. Res. 103, 9691–9712.

Boettcher, M.S., Jordan, T.H., 2004. Earthquake scaling relations for mid-ocean ridge transform faults. J. Geophys. Res. 109, B12302. doi:10.1029/2004JB003110.

Bourouis, S., Bernard, P., 2007. Evidence for coupled seismic and aseismic fault slip during water injection in the geothermal site of Soultz (France), and implications for seismogenic transients. Geophys. J. Int. 169, 723–732. doi:10.1111/j.1365-246X.2006.-03325.x.

Brodsky, E.E., Mori, J., 2007. Creep events slip less than ordinary earthquakes. Geophys. Res. Lett. 34, L16309. doi:10.1029/2007GL030917.

Brooks, B.A., Foster, J.H., Bevis, M., Frazer, L.N., Wolfe, C.J., Behn, M., 2006. Periodic slow earthquakes on the flank of Kilauea volcano, Hawai i, Earth Planet. Sci. Lett. 246, 207–216. doi:10.1016/j.epsl.2006.03.035.

Catalli, F., Cocco, M., Console, R., Chiaraluce, L., 2008. Modeling seismicity rate changes during the 1997 Umbria–Marche sequence (central Italy) through a rate- and state-dependent model. J. Geophys. Res. 113, B11301. doi:10.1029/2007JB005356.

Cervelli, P., Segall, P., Johnson, K., Lisowski, M., Miklius, A., 2002. Sudden aseismic fault slip on the south flank of Kilauea volcano. Nature 415, 1014–1018.

Chester, F.M., Higgs, N.G., 1992. Multimechanism friction constitutive model for ultrafine quartz gouge at hypocentral conditions. J. Geophys. Res. 97, 1859–1870.

Console, R., Murru, M., Catalli, F., 2006. Physical and stochastic models of earthquake clustering. Tectonophysics 417, 141–153. doi:10.1016/j.tecto.2005.05.052.

Console, R., Murru, M., Catalli, F., Falcone, G., 2007. Real time forecasts through an earthquake clustering model constrained by the rate-and-state constitutive law: comparison with a purely stochastic ETAS model. Seis. Res. Lett. 78, 49–56.

Dieterich, J., 1994. A constitutive law for rate of earthquake production and its application to earthquake clustering. J. Geophys. Res. 99, 2601–2618.

Dieterich, J., Cayol, V., Okubo, P., 2000. The use of earthquake rate changes as a stress meter at Kilauea volcano. Nature 408, 457–460.

Einarsson, P., Brandsdóttir, B., 1980. Seismological evidence for lateral magma intrusion during the July 1978 deflation of the Krafla volcano in NE-Iceland. J. Geophys. 47, 160–165.

Gross, S., Kisslinger, C., 1997. Estimating tectonic stress rate and state with Landers aftershocks. J. Geophys. Res. 102, 7603–7612.

Hainzl, S., Ogata, Y., 2005. Detecting fluid signals in seismicity data through statistical earthquake modeling. J. Geophys. Res. 110. doi:10.1029/2004JB003247.

Harris, R.A., Simpson, R.W., 1998. Suppression of large earthquakes by stress shadows: a comparison of Coulomb and rate-and-state failure. J. Geophys. Res. 103, 24439–24451.

Helmstetter, A., 2003. Is earthquake triggering driven by small earthquakes? Phys. Rev. Lett. 91. doi:10.1103/PhysRevLett.91.058501.

Helmstetter, A., Sornette, D., 2002. Subcritical and supercritical regimes in epidemic models of earthquake aftershocks. J. Geophys. Res. 107 (B10), 2237. doi:10.1029/2001JB001580.

Helmstetter, A., Sornette, D., 2003. Bath's law derived from the Gutenberg–Richter law and from aftershock properties. Geophys. Res. Lett. 30. doi:10.1029/2003GL018186.

Helmstetter, A., Shaw, B.E., 2006. Relation between stress heterogeneity and aftershock rate in the rate-and-state model. J. Geophys. Res. 111, B07304. doi:10.1029/2005JB004077.

Hill, D.P., Mowinckel, P., Peake, L.G., 1975. Earthquakes, active faults and geothermal areas in the Imperial Valley, California. Science 188, 1306–1308.

Kisslinger, C., Jones, L.M., 1991. Properties of aftershock sequences in southern California. J. Geophys. Res. 96, 11,947–11,958.

Lohman, R.B., McGuire, J.J., 2007. Earthquake swarms driven by aseismic creep in the Salton Trough, California. J. Geophys. Res. 112, B04405. doi:10.1029/2006JB004596.

McGuire, J.J., Boettcher, M.S., Jordan, T.H., 2005. Foreshock sequences and short-term earthquake predictability on East Pacific Rise transform faults. Nature 434. doi:10.1038/nature03377.

Mogi, K., 1962. Study of elastic shocks caused by the fracture of heterogeneous materials and its relation to earthquake phenomena. Bull. Earthquake Res. Inst. Univ. Tokyo 40, 125–173.

Mogi, K., 1967. Regional variation of aftershock activity. Bull. Earthquake Res. Inst. Univ. Tokyo 45, 711–726.

Ogata, Y., 1988. Statistical models for earthquake occurrences and residual analysis for point processes. J. Am. Stat. Assoc. 83, 9–27.

Ogata, Y., 1998. Space–time point-process models for earthquake occurrences. Ann. Inst. Statist. Math. 50, 379–402.

Ogata, Y., 2004. Space–time model for regional seismicity and detection of crustal stress changes. J. Geophys. Res. 109, B03308. doi:10.1029/2003JB002621.

Ogata, Y., 2005. Detection of anomalous seismicity as stress change sensor. J. Geophys. Res. 110, B05S06. doi:10.1029/2004JB003245.

Omori, F., 1894. On the aftershocks of earthquakes. J. Coll. Sci. Imp. Univ. Tokyo 7, 111–200.

Ozawa, S., Miyazaki, S., Hatanaka, Y., Imakiire, T., Kaidzu, M., Murakami, M., 2003. Characteristic silent earthquakes in the eastern part of the Boso peninsula, Central Japan. Geophys. Res. Lett. 30 (6), 1283. doi:10.1029/2002GL016665.

Ozawa, S., Suito, H., Tobita, M., 2007. Occurrence of quasi-periodic slow-slip off the east coast of the Boso peninsula, Central Japan. Earth Planets Space 59, 1241–1245.

Prejean, S., Stork, A., Ellsworth, W., Hill, D., Julian, B., 2003. High precision earthquake locations reveal seismogenic structure beneath Mammoth Mountain, California. Geophys. Res. Lett. 30 (24), 2247. doi:10.1029/2003GL018334.

Richter, C.F., 1958. Elementary Seismology. W.H. Freeman, San Francisco.

Sagiya, T., 2004. Interplate coupling in the Kanto district, central Japan, and the Boso peninsula silent earthquake in May 1996. Pure Appl. Geophys. 161. doi:10.1007/s00024-004-2566-6.

Segall, P., Desmarais, E.K., Shelly, D., Miklius, A., Cervelli, P., 2006. Earthquakes triggered by silent slip events on Kilauea volcano, Hawaii. Nature 442. doi:10.1038/nature04938.

Shapiro, S.A., Rentsch, S., Rothert, E., 2005. Characterization of hydraulic properties of rocks using probability of fluid-induced microearthquakes. Geophysics 70, F27–F33. doi:10.1190/1.1897030.

Smith, K.D., von Seggern, D., Blewitt, G., Preston, L., Anderson, J.G., Wernicke, B.P., Davis, J.L., 2004. Evidence for deep magma injection beneath Lake Tahoe, Nevada–California. Science 305. doi:10.1126/science.1101304.

Takada, Y., and Furuya, M., in review, Aseismic slip during the 1996 earthquake swarm in and around the Onikobe geothermal area, NE Japan, Earth Planet. Sci. Lett.

Toda, S., Matsumura, S., 2006. Spatio-temporal stress states estimated from seismicity rate changes in the Tokai region, central Japan. Tectonophysics 417, 53–68. doi:10.1016/j.tecto.2005.08.030.

Toda, S., Stein, R.S., Reasenberg, P.A., Dieterich, J.H., 1998. Stress transferred by the Mw = 6.5 Kobe, Japan, shock: effect on aftershocks and future earthquake probabilities. J. Geophys. Res. 103, 24,543–24,565.

Toda, S., Stein, R.S., Sagiya, T., 2002. Evidence from the AD 2000 Izu islands earthquake swarm that stressing rate governs seismicity. Nature 419, 58–61.

Utsu, T., 1961. A statistical study on the occurrence of aftershocks. Geophys. Mag. 30, 521–605.

Utsu, T., Ogata, Y., Matsu'ura, R.S., 1995. The centenary of the Omori formula for a decay law of aftershock activity. J. Phys. Earth 43, 1–33.

Vidale, J.E., Shearer, P.M., 2006. A survey of 71 earthquake bursts across southern California: exploring the role of pore fluid pressure fluctuations and aseismic slip as drivers. J. Geophys. Res. 111, B05312. doi:10.1029/2005JB004034.

Vidale, J.E., Boyle, K.L., Shearer, P.M., 2006. Crustal earthquake bursts in California and Japan: their patterns and relation to volcanoes. Geophys. Res. Lett. 33, L20313. doi:10.1029/2006GL027723.

Wessel, P., Smith, W.H.F., 1998. New, improved version of generic mapping tools released. Eos Trans. AGU 79 (47), 579.

Wolfe, C.J., Brooks, B.A., Foster, J.H., Okubo, P.G., 2007. Microearthquake streaks and seismicity triggered by slow earthquakes on the mobile south flank of Kilauea Volcano, Hawai i. Geophys. Res. Lett. 34, L23306. doi:10.1029/2007GL031625.